COHERENT STRUCTURES AND HEAT TRANSPORT IN TURBULENT RAYLEIGH-BÉNARD CONVECTION

Claus Wagner
Institute for Aerodynamics and Flow Technology,
German Aerospace Centre
Bunsenstr. 10, D-37073 Göttingen, Germany
claus.wagner@dlr.de

Olga Shishkina
Institute for Aerodynamics and Flow Technology,
German Aerospace Centre
Bunsenstr. 10, D-37073 Göttingen, Germany
olga.shishkina@dlr.de

ABSTRACT

Thermal plumes and their role for the heat transport in turbulent Rayleigh–Bénard convection of air (Prandtl number $Pr = 0.7$) in a cylindrical cell are investigated analysing data obtained from Direct Numerical Simulations (DNS) and well-resolved Large-Eddy Simulations (LES). DNS have been performed for the Rayleigh numbers $Ra = 10^6$ and 10^7 and aspect ratio of a cylindrical container $\Gamma = 5$ and LES for $Ra = 10^8$ and $\Gamma = 5$. Additionally a LES has been conducted for $Ra = 10^9$ and $\Gamma = 1$ to provide a high Rayleigh number flow field for a parametrized plume analysis. It is shown that the number of the thermal plumes increase with increasing Rayleigh numbers while their size decreases. Further, temperature thresholds are determined based on a thermal dissipation rate analysis, which are used for plume extraction.

INTRODUCTION

Buoyancy driven turbulent convection in fluid layers between a lower heated and a upper cooled plate which is usually denoted as Rayleigh–Bénard convection (RBC) has been the subject of a number of review articles, see for example Siggia (1994) or Bodenschatz et al. (2000). Recently, the global heat transport and its dependences on the Rayleigh number $Ra = \alpha g \hat{H}^3 \Delta\hat{T}/(\kappa\nu)$, Prandtl $Pr = \nu/\kappa$ number and aspect ratio of the container $\Gamma = \hat{D}/\hat{H}$ have been studied also theoretically by Otero et al. (2002) and Grossmann and Lohse (2004)), experimentally by Funfschilling et al. (2005) and du Puits et al. (2007) and in numerical simulation by Stringano and Verzicco (2006) and Shishkina and Wagner (2006). Above, α denotes the thermal expansion coefficient, ν the kinematic viscosity, κ the thermal diffusivity, g the gravitational acceleration, $\Delta\hat{T}$ the temperature difference between the bottom and the top plates, $\hat{H}$ the height and $\hat{D}$ the diameter of the Rayleigh-Bénard cell.

From flow visualizations of turbulent RBC it is known that large coherent structures develop which have mushroom-like form in the bulk viewing from the side and a sheetlike shape from above (Funfschilling and Ahlers, 2004). These structures are called the thermal plumes. Generally, these plumes are generated in the thermal boundary layers close to the bottom or the top plate and are driven to the opposite plate by buoyancy. It is also known that the sheetlike roots (or "mycelium theads") of the plumes are located at the borders between the boundary layers and the bulk or slightly deeper in the bulk (Shishkina and Wagner, 2006). The temperature of the thermal plumes differs significantly from the mean temperature of the background fluid. Due to the temperature difference between these large flow structures and the surrounding fluid (and, hence, due to different refractive indices in these parts of the fluid) the thermal plumes become visible.

Although the thermal plumes are identified easily by eye in experiments, the problem of their extraction is not satisfactorily solved. Thresholds of certain quantities, i.e. the temperature (Zhou and Xia, 2002) and/or the vertical component of the velocity field (Juliem et al., 1999), the skewness of the temperature derivative (Belmonte and Libhacher, 1996) or the local thermal dissipation rate (Shishkina and Wagner, 2006) have been usually used for plume identification so far. But to properly determine a threshold value which separates the large coherent structures from the background fluid is still an unsolved problem.

In the present paper we suggest a new way to investigate the sheet-like thermal plumes based on time-dependent three-dimensional flow fields which we generated in Direct Numerical Simulations (DNS) or well-resolved Large-Eddy Simulations (LES) of turbulent RBC. In our study temperature thresholds for thermal plumes extraction are determined in a thermal dissipation rate analysis. To demonstrate the ability of our approach we present thermal plumes extracted from LES data of RBC in air ($Pr = 0.7$) for the Rayleigh number $Ra = 10^9$ and the aspect ratio of the cylindrical domain $\Gamma = 1$.

Further, we analyze the correlation between these plumes and the local heat fluxes for various Rayleigh numbers to improve the understanding of the role of those plumes for and the dependences of the Rayleigh number on the global heat transport.

GOVERNING EQUATIONS

The governing dimensionless momentum, energy and continuity equations for the considered Rayleigh-Bénard problem read

$$\begin{aligned}
\mathbf{u}_t + \mathbf{u}\cdot\nabla\mathbf{u} + \nabla p &= \Gamma^{-3/2} Ra^{-1/2} Pr^{1/2} \Delta\mathbf{u} + T\mathbf{e}_z, \\
T_t + \mathbf{u}\cdot\nabla T &= \Gamma^{-3/2} Ra^{-1/2} Pr^{-1/2} \Delta T, \qquad (1)\\
\nabla\cdot\mathbf{u} &= 0.
\end{aligned}$$

with the dimensionless variables $\mathbf{u}$ the velocity vector-function, T the temperature, $\mathbf{u}_t$ and T_t their time derivatives and p the pressure as well as the unit vector in vertical direction $\mathbf{e}_z$. To obtain these equations the reference velocity $\hat{u}_{ref} = \left(\alpha g \hat{D}\,\Delta\hat{T}\right)^{1/2}$ and the refence length $\hat{x}_{ref} = \hat{D}$ have been applied. The dimensionless temperature varies between $T|_{z=0} = +0.5$ at the bottom and $T|_{z=H} = -0.5$ at the top horizontal walls and satisfies $\partial T/\partial\mathbf{n} = 0$ on the vertical walls, where $\mathbf{n}$ is the normal vector. On the boundary the velocity field vanishes, i.e. $\mathbf{u}|_{\partial\Upsilon} = 0$.

To discretize equations (1) with respect to time we use the leapfrog scheme for the convective terms $\mathbf{u}\cdot\nabla\mathbf{u}$ and $\mathbf{u}\cdot\nabla T$ and Euler-forward scheme for the diffusive terms $\Delta\mathbf{u}$ and ΔT as presented in Shishkina and Wagner (2004) while spatial discretizition of equations (1) is based on a finite volume approach. For any component of the velocity vector in β-direction the equation (1) averaged for any finite volume V reads

$$\frac{\left\langle u_\beta^{n+1}\right\rangle_V - \left\langle u_\beta^{n-1}\right\rangle_V}{2\Delta t} + \left\langle \mathbf{u}^n\cdot\nabla u_\beta^n\right\rangle_V + \left\langle \nabla p^n\cdot\mathbf{e}_\beta\right\rangle_V = \left\langle \mu\Delta u_\beta^{n-1}\right\rangle_V + \left\langle T^n\right\rangle_V \delta_z^\beta,$$

where $<\cdot>_V$ denotes averaging over a finite volume V and δ_z^β the Kronecker symbol. Using Gauß–Ostrogradsky theorem and the continuity equation, we reduce the convective and diffusive terms in this equation to the following surface integrals

$$\left\langle \mathbf{u}^n\cdot\nabla u_\beta^n\right\rangle_V = \left\langle \nabla\cdot(u_\beta^n\mathbf{u}^n)\right\rangle_V - \left\langle u_\beta^n\nabla\cdot\mathbf{u}^n\right\rangle_V = \frac{1}{|V|}\oint_S \mathbf{n}\cdot\left(u_\beta^n\mathbf{u}^n\right)\,dS, \tag{2}$$

$$\left\langle \mu\Delta u_\beta^{n-1}\right\rangle_V = \mu\left\langle \nabla\cdot\nabla u_\beta^{n-1}\right\rangle_V = \frac{\mu}{|V|}\oint_S \mathbf{n}\cdot\nabla u_\beta^{n-1}\,dS, \tag{3}$$

In (2) and (3) $|V|$ denotes the size and S the surface of the finite volume V. Further, Δt stands for the time step, the subscript n for the number of the considered time level, Δ_φ for the second order partial derivative in the azimuthal direction φ and $\mu = \Gamma^{-3/2}Ra^{-1/2}Pr^{1/2}$. The discretization schemes for the energy equation are constructed analogously. The surface averaged quantities in (2), (3) are computed from the volume averages ones using the fourth-order approximation schemes in cylindrical coordinates presented in Shishkina and Wagner (2005, 2007).

SUBGRID SCALE MODELING AND MESH RESOLUTION

To compute the convective term (2) we need to approximate $\langle u_i u_j\rangle_S$ based on the velocity values $\langle u_i\rangle_S$, where $<\cdot>_S$ denotes averaging over any surface S. For DNS the first term of the Fourier series

$$\langle u_i u_j\rangle_S = \langle u_i\rangle_S \langle u_j\rangle_S + \frac{1}{12}\sum_\beta \Delta\beta^2 \frac{\partial\langle u_i\rangle_S}{\partial\beta}\frac{\partial\langle u_j\rangle_S}{\partial\beta} + \mathcal{O}\left(\sum_\beta \Delta\beta^4\right)$$

is used to compute $\langle u_i u_j\rangle_S$. Here $\Delta\beta$ is the mesh size in the β-direction. For LES the second term is additionally used according to the tensor diffusivity subgrid-scale model by Leonard and Winkelmans (1999).

The conducted DNS ($Ra = 10^6$ and $Ra = 10^7$, $\Gamma = 5$) and LES ($Ra = 10^8$, $\Gamma = 5$) were performed on staggered grids with $110\times512\times192$ points in the vertical, azimuthal and radial directions, respectively, while the mesh used for the LES for $Ra = 10^9$ and $\Gamma = 1$ consists of $220\times512\times96$ nodes. The grid points are distributed equidistantly in the azimuthal direction and are clustered in the vicinity of the rigid walls to resolve the viscous and thermal boundary layers. Thus, close to the horizontal plates the size of the finite volumes in the vertical direction is not more than 3.5%, 6.7% and 14.1% of the corresponding thermal boundary layer thickness

$$\lambda_\theta(Ra) = H/(2Nu)$$

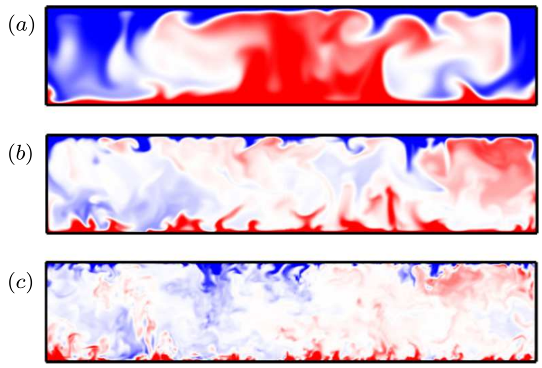

Figure 1: Vertical distributions of the instantaneous temperature field $-0.5\le T\le 0.5$ for the Rayleigh numbers $Ra = 10^6$ (a), 10^7 (b), 10^8 (c) and $\Gamma = 5$. The grey (color) scale ranges from black (blue) for $T\le -0.3$ through white ($T = 0$) to grey (red) for $T\ge 0.3$.

for the cases $Ra = 10^6$, $Ra = 10^7$ and $Ra = 10^8$, respectively, where

$$Nu = \Gamma^{1/2}Ra^{1/2}Pr^{1/2} < u_z T >_{t,V} + 1, \tag{4}$$

symbolizes the Nusselt number and $<\cdot>_{t,V}$ time- and volume-averaging.

The computational mesh used in the DNS for $Ra = 10^6$ and $Ra = 10^7$ is fine enough to resolve all relevant turbulent scales, if the mean width $h_{V_i} = (\Delta z_i\, r_i\Delta\varphi_i\,\Delta r_i)^{1/3}$ of any finite volume V_i satisfies the inequality

$$h_{V_i} \le \pi\eta_{V_i}(Ra), \tag{5}$$

where $\eta_{V_i}(Ra)$ is the Kolmogorov scale at the location of the finite volume V_i. For the dimensionless system (1) the Kolmogorov scale equals

$$\eta_{V_i}(Ra) = \mu_1^{3/4} < \epsilon_u >_{t,\varphi}^{-1/4} \tag{6}$$

and depends on the vertical and radial coordinates, z and r. Here ϵ_u is the turbulent kinetic energy dissipation rate and $<\cdot>_{t,\varphi}$ denotes averaging in time and in the azimuthal φ-direction. It is well-known that the turbulent kinetic energy dissipation rate peaks in the close vicinity of the rigid walls. In these regions the Kolmogorov scale and, hence, the mesh width are small, while in the the bulk they are larger. Evaluating the values of $<\epsilon_u>_{t,\varphi}$ and η_{V_i} from the DNS data for the cases $Ra = 10^6$ and 10^7 we obtain

$$\pi^{-1}\max_{V_i}\{h_{V_i}\eta_{V_i}^{-1}(10^6)\} \le 0.41,$$
$$\pi^{-1}\max_{V_i}\{h_{V_i}\eta_{V_i}^{-1}(10^7)\} \le 0.81.$$

Therefore it is concluded that the computational mesh used in the DNS satisfies the resolution requirements both in the bulk and in the vicinity of the walls. It must be further noted that even for the LES, which we performed for $Ra = 10^9$, we obtain

$$\pi^{-1}\max_{V_i} h_{V_i}\eta_{V_i}^{-1}(10^9) \le 1.56$$

indicating that this simulation is also well-resolved.

INSTANTANEOUS AND MEAN FLOW FIELDS

In Fig. 1 and Fig. 2 snapshots of the temperature fields in vertical and horizontal planes highlight the complex three-dimensional thermal plumes which are generated in the thermal boundary layers and are driven by buoyancy. With growing Rayleigh number the characteristic size of these plumes decreases while their number increases. The distribution of the instantaneous temperature fields in

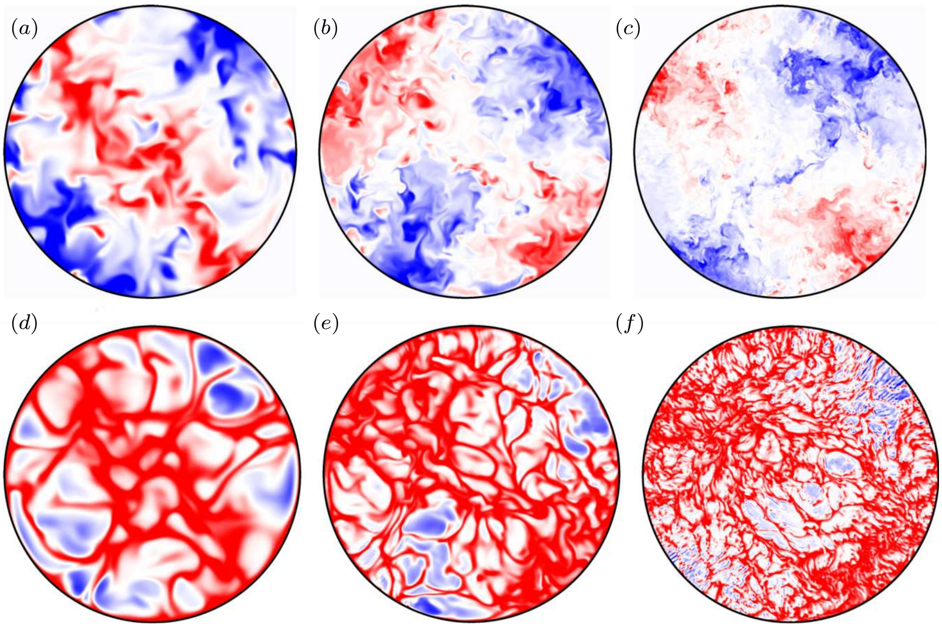

Figure 2: Horizontal distributions of the instantaneous temperature field $-0.5 \leq T \leq 0.5$ for $z = 0.5H$ $(a-c)$ and $z = H/(2Nu)$ $(d-f)$ and the Rayleigh numbers $Ra = 10^6$ (a, d), 10^7 (b, e), 10^8 (c, f) and $\Gamma = 5$. The grey scale (color) scale ranges from black (blue) for $T \leq -0.3$ through white ($T = 0$) to grey (red) for $T \geq 0.3$.

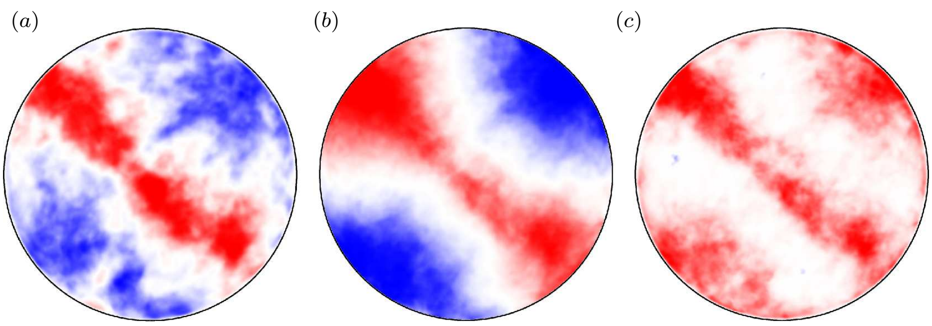

Figure 3: Horizontal distributions of the mean axial velocity $< u_z >_t$ (a), the mean temperature $< T >_t$ (b) and the mean convective heat flux $< u_z T >_t$ (c) in the center horizontal cross-section for $z = H/2$, $Ra = 10^7$ and$\Gamma = 5$. The grey (color) scale ranges from black (blue) for negative values, through white (zero) to grey (red) for positive values.

Fig. 2 $(d-f)$ in a horizontal plane located close to the heated bottom plate reflect large scale structures denoted in Shishkina and Wagner (2006) as the roots of the thermal plumes. Increasing the Rayleigh number (Fig. 2 (d) to Fig. 2 (f)) these roots become thinner and their number increases.

For the statistical analysis time-averaging $< \cdot >_t$ was performed for more than 43, 110 and 59 dimensionless time units for Ra equals 10^6, 10^7 and 10^8, respectively. For $Ra = 10^7$ and $z = H/2$ the time-averaged fields of the temperature $< T >_t$, axial velocity $< u_z >_t$ and the vertical convective heat transport $< u_z T >_t$ are presented in Fig. 3. For the case of the presented Ra-number $Ra = 10^7$ the mean flow rises through a diametral stripe and descends in two regions close to the vertical wall. Contrary to this, for the lower Rayleigh number ($Ra = 10^6$) the mean flow is organized in more rolls, while a convection cell with upflow in the center is obtained for the higher Rayleigh number $Ra = 10^8$ (not shown).

INSTANTANEOUS AND MEAN HEAT FLUXES

Although both, the time- and/or horizontal area-averaging in cross-section S_z of the heat fluxes leads to the same Nusselt number Nu, the local heat flux

$$\Omega = \Gamma^{1/2} Ra^{1/2} Pr^{1/2} u_z T - \Gamma^{-1} \frac{\partial T}{\partial z} \tag{7}$$

is varying in space and in time. A perspective view of heat flux iso-surfaces obtained for $Ra = 10^6$ is presented in Fig. 4. It is observed

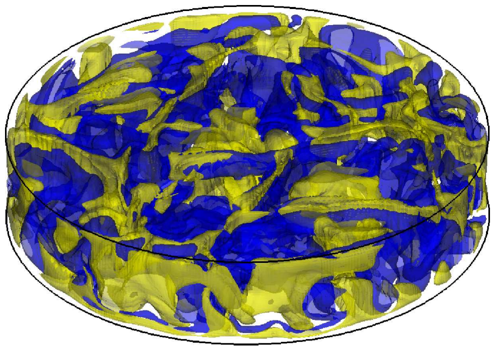

Figure 4: Regions of negative ($\Omega < 0$, dark grey (blue)) and large positive ($\Omega \geq 2Nu$, bright grey (yellow)) local heat flux values Ω obtained for $Ra = 10^6$ and $\Gamma = 5$.

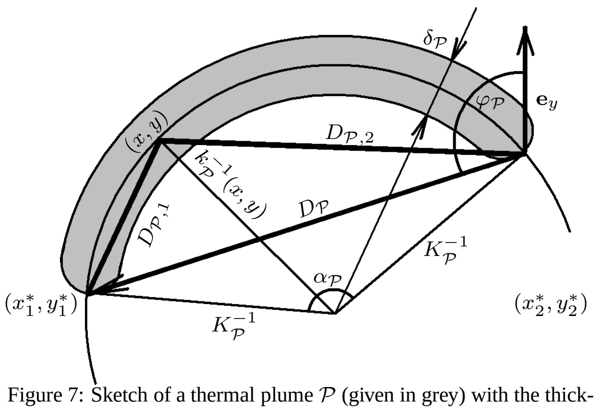

Figure 7: Sketch of a thermal plume $\mathcal{P}$ (given in grey) with the thickness $\delta_{\mathcal{P}}$, diameter $D_{\mathcal{P}}$, curvature $K_{\mathcal{P}}$ and plume angle $\varphi_{\mathcal{P}}$.

that a large part of the domain is characterized by high ($\geq 2Nu$) local heat flux values Ω but in up to one third of the Rayleigh-Bénard cells volume the local heat fluxes are negative.

Evaluating thze global heat flux in terms of the Nusselt numbers (4) leads to $Nu = 8.16$ for $Ra = 10^6$, $Nu = 15.54$ for $Ra = 10^7$, $Nu = 32.95$ for $Ra = 10^8$ and $Nu = 67.07$ for $Ra = 10^9$. These values are in good agreement with those obtained by Niemela et al. (2000) and by Wu and Libchaber (1992), who reported $Nu = 0.124 Ra^{0.309}$ for $\Gamma = 0.5$ and $Nu = 0.147 Ra^{0.287}$ for $\Gamma = 6.7$, respectively.

Further, we investigate the spatial distribution of the instantaneous heat fluxes using the DNS and LES data. In Fig. 5 contours of the instantaneous vertical heat fluxes are plotted together with superimposed velocity vectors for $Ra = 10^7$ and different distances from the bottom plate.

In the center horizontal cross-section (Fig. 5*a*) regions of high values of Ω correspond to fluid moving predominantly in vertical directions (indicated by the velocity arrows, which reduce to dots in Fig. 5*a*). These regions are zones of clustered plume stems (see Shishkina and Wagner, 2006) around which the fluid can move rotationally.

In the vicinity of the bottom plates (Fig. 5 *c*), regions with comparably large values of the local heat flux Ω are observed mainly near the vertical wall, where the fluid moves from the centers of cold plume caps in all possible horizontal directions. At the borders between the thermal boundary layers and the bulk (Fig. 5*b*), fluid which is characterized by high local heat flux values can move in both, the horizontal directions (like in near the horizontal wall region in Fig. 5*c*) and in the vertical directions (like in the center horizontal cross-section in Fig. 5*a*)).

Comparing the snapshots of the local heat flux in Fig. 5, which are taken at different distances from the horizontal and vertical walls, one concludes that the presense of the rigid walls influences significantly the spatial distribution of the instantaneous heat flux.

SHEETLIKE THERMAL PLUMES EXTRACTION

To investigate sheetlike thermal plumes a LES of turbulent Rayleigh-Bénard convection of air (Prandtl numer $Pr = 0.7$) for $Ra = 10^9$ has been performed since for this high Rayleigh number the plumes are difficult to detect visually.

Snapshots of the temperature field (Fig. 5*a*) and the thermal dissipation rate (Fig. 5*b*) in a horizontal plane located at the border between the upper cold thermal boundary layer and the bulk ($z = 0.5H/Nu$) give an impression of the characteristic three-dimensional flow structures of turbulent RBC.

To determine the temperature threshold which separates the thermal plumes from the background fluid we investigate the temperature dependences of the thermal dissipation rate. For a fixed horizontal

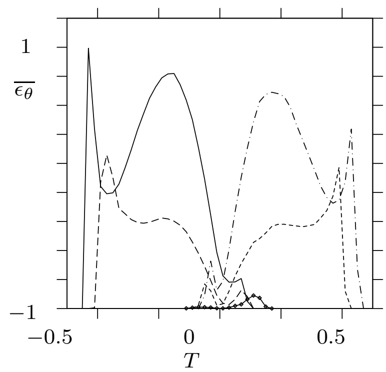

Figure 8: Distribution of the thermal dissipation rate evaluated for $Ra = 10^9$, $Pr = 0.7$, $\Gamma = 1$ and distances $z = 0.5H/Nu$ (——), $z = H/Nu$ (– – –), $z = H/2$ (–•–), $z = H(1 - 1/Nu)$ (- - -) $z = H(1 - 0.5/Nu)$ (– · –) from the top plate.

cross-section S_z within the cylindrical Rayleigh-Bénard cell and temperature values within a given interval $[T_k, T_{k+1}[$ we calculate the thermal dissipation rate $\overline{\epsilon_\theta}$ as follows

$$\overline{\epsilon_\theta} = C_{\epsilon_\theta} \left\langle \epsilon_\theta \; \vartheta(T_k \leq T < T_{k+1}) \right\rangle_{t, S_z},$$

where $\theta(T_k \leq T \leq T_{k+1}) = \mathcal{H}(T - T_k) - \mathcal{H}(T - T_{k+1})$ with $\mathcal{H}(x)$ the Heaviside function and the normalizing constant C_{ϵ_θ}.

In Fig. 8 the obtained values of the thermal dissipation rate (evaluated for $Ra = 10^9$, $Pr = 0.7$, $\Gamma = 1$) are presented for different distances from the top plate. Large absolute values of the temperature in Fig. 8 are associated with interior of the thermal plumes, while those around zero correspond to the background fluid. The borders between the thermal boundary layers and the bulk ($z = 0.5H/Nu$ and $z = H(1 - 0.5/Nu)$) are the most interesting regions, since there the sheetlike plumes develop. Solid lines in Fig. 8 correspond to $z = 0.5H/Nu$. It is observed that within the temperature interval $-0.4 \leq T \leq 0$ the thermal dissipation rate (Fig. 8 *d*) has a well-pronounced extermum which corresponds to the temperature threshold T_{thr}^- used to extract the sheetlike plumes at the border between the upper cold thermal boundary layer and the bulk.

GEOMETRICAL PROPERTIES OF SHEETLIKE PLUMES

In the horizontal cross-sections S_z located at $z = H(1 - 0.5/Nu)$ and $z = 0.5H/Nu$ from the top plate, warm and cold sheetlike thermal plumes are identified as subdomains of S_z, restricted by the plume temperature thresholds T_{thr}^+ and T_{thr}^-, as follows

$$\mathcal{P}^+ = \{(\mathbf{x}) \in S_z : T(\mathbf{x}) \in [T_{thr}^+, 0.5]\},$$
$$\mathcal{P}^- = \{(\mathbf{x}) \in S_z : T(\mathbf{x}) \in [-0.5, T_{thr}^-]\}.$$

Here the vertical coordinate z and time t are omitted and $\mathbf{x} = (x, y)$. In Fig. 5(c) the cold sheetlike plumes, which were extracted at the border between the upper themal boundary layer and the bulk (with a distance $z = 0.5H/Nu$ from the top plate), are presented. The corresponding snapshot of the temperature field is shown in Fig. 5(a).

In our plume analysis we neglect those thermal plumes with a relative area

$$A_{\mathcal{P}} = |\mathcal{P}|/|S_z|$$

of less than 2×10^{-4}, where $|\mathcal{P}|$ and $|S_z|$ denote the areas of $\mathcal{P}$ and S_z, respectively. The plume diameter $D_{\mathcal{P}}$ is defined as the maximum distance between any two points in $\mathcal{P}$, and varies between 0 and 1 (see Fig. 7 for a schematic sketch of a sheetlike thermal plume and its geometrical characteristics).

The plume vector $\mathbf{a}_{\mathcal{P}} = \left(x_1^* - x_2^*, y_1^* - y_2^*\right)$ of the length $D_{\mathcal{P}}$ has a direction such that $\mathbf{e}_y \times \mathbf{a}_{\mathcal{P}}$ points upwards, for $\mathbf{e}_y$ being the unit vector in the y-direction. Thus, the angle $\varphi_{\mathcal{P}}$ between the plume vector $\mathbf{a}_{\mathcal{P}}$ and the unit ordinate vector $\mathbf{e}_y$ varies in the interval $[0, \pi]$.

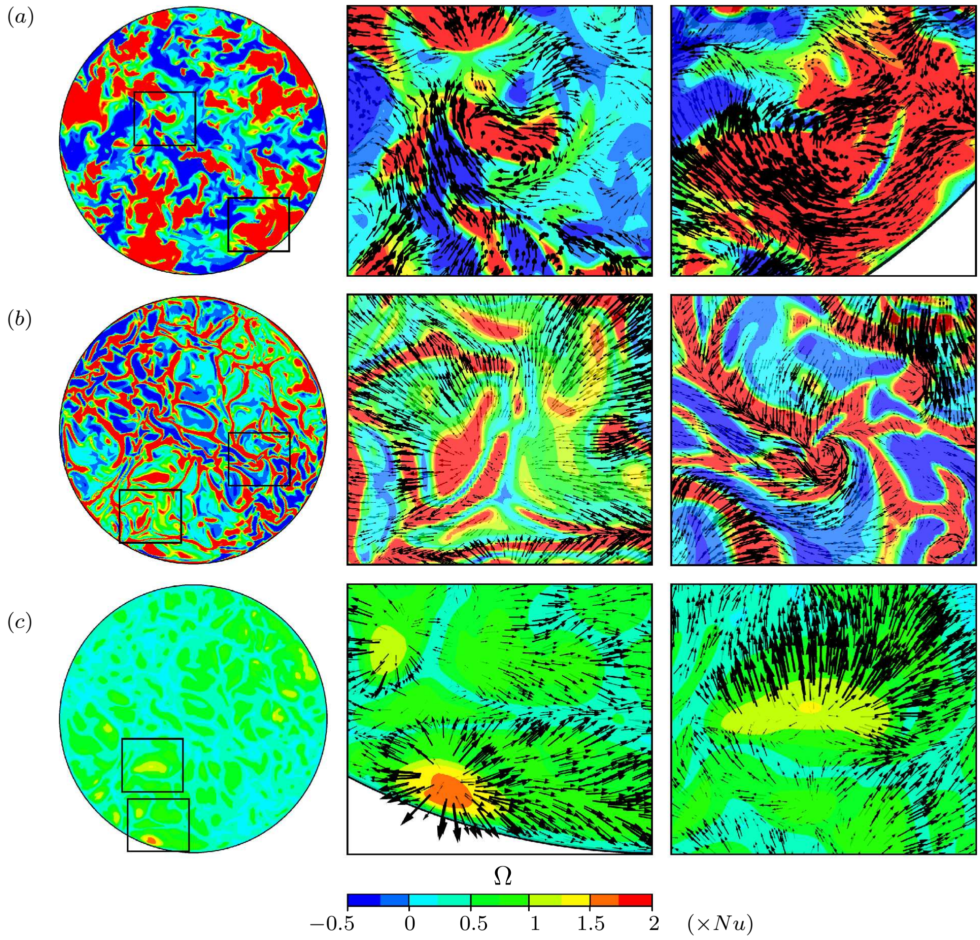

Figure 5: Snapshots of local heat fluxes obtained for $Ra = 10^7$, $Pr = 0.7$, $\Gamma = 5$ and $z = 0.5H$ (a), $z = H/(2Nu)$ (b) and $z = 10^{-3}H$ (c). Close-up views with superimposed velocity vectors are presented on the right.

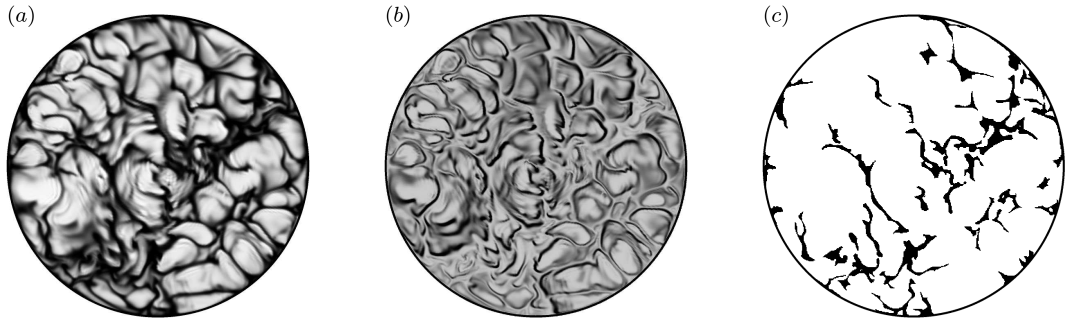

Figure 6: Snapshots of the temperature field (a), the thermal dissiaption rate (b) and extracted thermal plumes (c) in the horizontal cross-section $z = 0.5H/Nu$ obtained for $Ra = 10^9$, $Pr = 0.7$ and $\Gamma = 1$. The grey scale ranges from black (negative values in (a) and positive values in (b)) to white (positive values in (a) and zero in (b)).

The plume direction and its diameter are determined, respectively, by the direction and the length of the vector $\mathbf{a}_\mathcal{P}$.

To determine the curvature of the plume $\mathcal{P}$ we consider each non-degenerate triangle with the vertexes $(x, y) \in \mathcal{P}$, $\left(x_1^*, y_1^*\right)$ and $\left(x_2^*, y_2^*\right)$ and the side lengths $D_\mathcal{P}$ and

$$D_{\mathcal{P},\beta} = \left((x_\beta^* - x)^2 + (y_\beta^* - y)^2\right)^{1/2}, \quad \beta = 1, 2.$$

The plume curvature $K_\mathcal{P}$,

$$K_\mathcal{P} = |\mathcal{P}|^{-1} \int_\mathcal{P} k_\mathcal{P}(x, y)\, d\mathcal{P},$$

is defined then as the quantity $k_\mathcal{P}(x, y)$ averaged over the sheetlike plume $\mathcal{P}$, where the value of $k_\mathcal{P}(x, y)$ is inversely proportional to the circumradius of the considered triangle,

$$\begin{aligned} |k_\mathcal{P}(x, y)| \quad = \quad & D_\mathcal{P}^{-1} D_{\mathcal{P},1}^{-1} D_{\mathcal{P},2}^{-1} \left(\left(D_\mathcal{P} + D_{\mathcal{P},1} + D_{\mathcal{P},2}\right)\right. \\ & \left(-D_\mathcal{P} + D_{\mathcal{P},1} + D_{\mathcal{P},2}\right) \times \\ & \left(D_\mathcal{P} - D_{\mathcal{P},1} + D_{\mathcal{P},2}\right) \\ & \left.\left(D_\mathcal{P} + D_{\mathcal{P},1} - D_{\mathcal{P},2}\right)\right)^{1/2}. \end{aligned}$$

The quantity $k_\mathcal{P}(x, y)$ is positive only if the point (x, y) is situated on the right of the plume vector $\mathbf{a}_\mathcal{P}$, i.e. $(x_1^* - x_2^*)(y - y_2^*) < (x - x_2^*)(y_1^* - y_2^*)$, and non-positive otherwise.

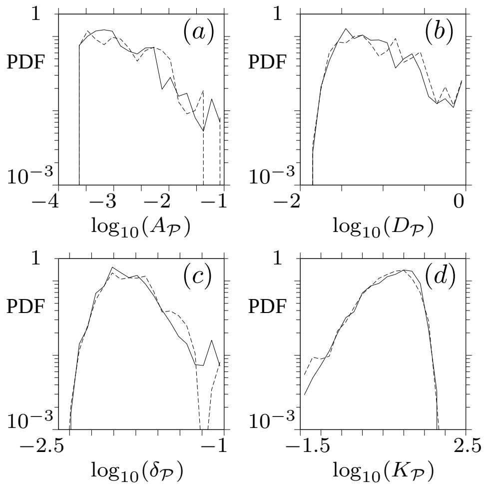

Figure 9: Probability density functions of the logarithms of the following geometrical characteristics of the thermal plumes: area (a), diameter (b), thickness (c) and curvature (d), evaluated for $Ra = 10^9$, $Pr = 0.7$, $\Gamma = 1$ and distances $z = 0.5H/Nu$ (——) and $z = H(1 - 0.5/Nu)$ (– – –) from the top plate.

Generally, the absolute value of the plume curvature $K_{\mathcal{P}}$ does not exceed $2D_{\mathcal{P}}^{-1}$. The curvature of a straight-line plume equals zero, while that of a plume with the shape replicating the boundary of the horizontal cross-section S_z equals ± 2.

Further, we consider the apical angle $\alpha_{\mathcal{P}}$ of the isosceles triangle with the vertexes $\left(x_1^*, y_1^*\right)$, $\left(x_2^*, y_2^*\right)$ and the circumcenter of the considered plume. Then the plume thickness $\delta_{\mathcal{P}}$ and the plume length $l_{\mathcal{P}}$ are defined as follows

$$\delta_{\mathcal{P}} = \alpha_{\mathcal{P}}^{-1} K_{\mathcal{P}} |\mathcal{P}|, \quad l_{\mathcal{P}} = \alpha_{\mathcal{P}} K_{\mathcal{P}}^{-1},$$

where the apical angle $\alpha_{\mathcal{P}}$ equals

$$\alpha_{\mathcal{P}} = \arccos\left(1 - \frac{(K_{\mathcal{P}} D_{\mathcal{P}})^2}{2}\right).$$

In Fig. 9 the probability density functions of the logarithms of the plume area, diameter, curvature, thickness and aspect ratio evaluated for $Ra = 10^9$, $Pr = 0.7$, $\Gamma = 1$ and distances $z = 0.5H/Nu$ and $z = H(1 - 0.5/Nu)$ from the top plate are presented. It is shown that the defined geometeric properties are reasonably distributed in turbulent RBC.

CONCLUSIONS

Analysing DNS- and LES-data of Rayleigh-Bénard convection for $Ra = 10^6$, 10^7 and 10^8, Prandtl number $Pr = 0.7$ and aspect ratio $\Gamma = 5$, it was shown that the number of thermal plumes increases with the Rayleigh number while their size decreases. These plumes play an important role for the heat transport. In regions of high values of the local heat flux in the vicinity of the bottom or the top plates (Fig. 5 c) the fluid moves predominantly from the centers of thermal plume caps towards their borders in all possible horizontal directions, while in the center horizontal cross-section (Fig. 5 a) these regions correspond to the vertical movement of the fluid through the plume stems around which the fluid can move rotationally.

Further, a new method for plume extraction and a way to parametrize these plumes was presented and tested analysing LES data of RBC for $Ra = 10^9$, $Pr = 0.7$ and $\Gamma = 1$.

ACKNOWLEDGEMENTS

The authors are grateful to the Deutsche Forschungsgemeinschaft (DFG) for financial supporting this work under the contract WA 1510.

REFERENCES

Bodenschatz, E., Pesch, W. and Ahlers, G. 2000, ”Recent developments in Rayleigh-Bénard convection”, *Annu. Rev. Fluid Mech.*, Vol. 32, pp. 709.

Belmonte, A., Libchaber, A., 1996, ”Thermal signature of plumes in turbulent convection: The skewness of the derivative”, *Phys. Rev. E*, Vol. 53, pp. 4893-4898.

du Puits, R., Resagk, C., Tilgner, A., Busse, F. H. and Thess, A., 2007, ”Structure of thermal boundary layers in turbulent Rayleigh-Bénard convection”, *J. Fluid Mech.*, Vol. 572, pp. 231-254.

Funfschilling, D., Ahlers, G., 2004, ”Plume motion and large-scale circulation in a cylindrical Rayleigh–Bénard cell”, *Phys. Rev. Lett.*, Vol. 92, pp. 494-502.

Funfschilling, D., Brown, E., Nikolaenko, A. and Ahlers, G., 2005, ”Heat transport by turbulent Rayleigh–Bénard convection in cylindrical samples with aspect ratio one and larger”, *J. Fluid Mech.*, Vol. 536, pp. 145-154.

Grossmann, G. and Lohse, D., 2004, ”Fluctuations in turbulent Rayleigh–Bénard convection: The role of plumes”, *Phys. Fluids*, Vol. 16, pp. 4462-4472.

Juliem, K., Legg, S., McWilliams, J., Werne, J., 1999, ”Plumes in rotating convection. Part 1. Ensemble statistics and dynamical balances”, *J. Fluid Mech.*, Vol. 391, pp. 151-187.

Leonard, A., Winckelmans, G. S., 1999, ”A tensor-diffusivity subgrid model for Large-Eddy Simulation”, *Caltech ASCI technical report*, cit-asci-tr043, Vol. 043.

Niemela, J. J., Skrbek, L., Sreenivasan, K. R. and R. J. Donnely, R. J., 2000, ”Turbulent convection at very high Rayleigh numbers”, *Nature*, Vol. 404, pp. 837-841.

Otero, J., Wittenberg, R. W., Worthing, R. A. and Doering, C. R., 2002, ”Bounds on Rayleigh–Bénard convection with an imposed heat flux”, *J. Fluid Mech.*, Vol. 473, pp. 191-199.

Shishkina, O. and Wagner, C., 2004, ”Stability conditions for the Leapfrog–Euler scheme with central spatial discretization of any order”, *Appl. Numer. Anal. and Comput. Math.*, Vol. 1, pp. 315-326.

Shishkina, O. and Wagner, C., 2005, ”A fourth order accurate finite volume scheme for numerical simulations of turbulent Rayleigh–Bénard convection”, *C. R. Mecanique*, Vol. 333, pp. 17-28.

Shishkina, O. and Wagner, C., 2006, ”Analysis of thermal dissipation rates in turbulent Rayleigh–Bénard convection”, *J. Fluid Mech.*, Vol. 546, pp. 51-60.

Shishkina, O. and Wagner, C., 2007, ”A fourth order finite volume scheme for turbulent flow simulations in cylindrical domains”, *Computers and Fluids*, Vol. 36 (2), pp. 484-497.

Siggia, E. D., 1994, ”High Rayleigh number convection”, *Ann. Rev. Fluid Mech.*, Vol. 26, pp. 137-168.

Stringano, G. and Verzicco, R., 2006, ”Mean flow structure in thermal convection in a cylindrical cell of aspect ratio one half”, *J. Fluid Mech.*, Vol. 548, pp. 1-16.

Wu, X.-Z. and Libchaber, A., 1992, ”Scaling relations in thermal turbulence: The aspect-ratio dependence”, *Phys. Rev. A*, Vol. 45, pp. 842-845.

Zhou, S.-Q., Xia K.-Q., 2000, ”Plume statistics in thermal turbulence: mixing of an active scalar”, *Phys. Rev. Lett.*, Vol. 89, pp. 484-502.